Arch. Metall. Mater. **62** (2017), 4, 2001-2006

DOI: 10.1515/amm-2017-0298

S. ISLAK*#

WEAR CHARACTERISTICS OF FeW/FeW-B_4C COATINGS PRODUCED BY TIG PROCESS

In this study, wear properties of FeW-B_4C coatings produced by tungsten inert gas (TIG) process on the AISI 1060 steel were investigated. TIG process was selected because it is a cost-effective approach for melting-based coatings. The treated surfaces were evaluated and characterized by means of scanning electron microscope (SEM), X-ray diffraction analysis, and electron dispersive spectrometry (EDS). The microhardness and wear experiment were also performed by using a microhardness machine and ball-on-disk tribometer. SEM observations showed that the obtained coating had a smooth and uniform surface. According to XRD analysis, borides and carbides phases formed in the coatings. The wear behavior of the coatings was compared with ball-on-disc configuration wear tests, at the same conditions. Average coefficient of friction values of the coatings were obtained at relatively low levels.

Keywords: Wear, coating, microstructure, TIG process

1. Introduction

Hardfacing process is a technique used to enhance surface properties of metallic materials such as hardness, wear and corrosion resistance at elevated temperature. These techniques using high energy density sources such as the plasma transferred arc (PTA) weld-surfacing process, tungsten inert gas (TIG) weld-surfacing and laser cladding (LC) have been commonly applied in order to enhance the mechanical, corrosion and tribological properties of the surfaces of components [1-3]. Among the weld cladding procedures, tungsten inert gas (TIG) surfacing process is a cost-effective approach applied when reactive materials (as coatings or substrates) are involved [4,5]. In weld-surfacing processes, both alloy powders and the surface of base metal are simultaneously melted and solidified to form a clad layer. The melted base metal will change the chemical composition and properties of the clad coatings. [6]. Rapidly solidified fine grain microstructure containing finely distributed hard carbide phases give rise to a surface coating having excellent combination of hardness, toughness, mechanical, corrosion or tribological properties [7].

In the materials science, composite coating is generally made up from a ductile matrix and ceramic reinforcement [8]. While nickel, cobalt, iron and titanium based alloys are used as matrix in the production of these composite coatings, in terms of reinforcement elements, hard reinforcement particles such as SiC, TiC, B_4C, WC, TiB_2 and Cr_3C_2 are preferred [9-17]. Recently, the application of B_4C in the surface coating pocesses has attracted more and more attentions for its super hardness, thermal stability, high melting point (2450 °C), low density (2.52 g/cm^3) and super mechanical properties [18]. Boron carbide (B_4C) is one of the hardest materials known, ranking third behind diamond and cubic boron nitride (cBN). Due to its high hardness, boron carbide powder is used as an abrasive material and it shows perfect wear resistance [19-21]. In this research, the processing of hard surfaces was done as B_4C particles mixed with FeW powders, and deposited by tungsten inert gas (TIG) weld-surfacing process. Coating layers are characterized using scanning electron microscopy (SEM) combined with EDS microanalysis, X-ray diffraction (XRD) and microhardness. The wear behavior of the coatings was compared with ball-on-disc configuration wear tests.

2. Experimental details

AISI 1060 steel (0.60 wt.% C, 0.67 wt.% Mn, 0.22 wt.% Si, 0.19 wt.% Ni and balance wt.% Fe) with dimensions 20 mm × 10 mm × 80 mm was used as the substrate material. In order to place coating powders, holes with 8 mm of width and 1,5 mm of depth were drilled on substrates. FeW powder was modified by addition of B_4C particles. B_4C particles were added to the powder alloys used for obtaining coating layers, in a rate of 10 wt.%. The average sizes of the FeW powder were from 10 to 75 μm, and the B_4C particles were less than 10 μm. Before TIG method, surfaces of steel material were cleaned with acetone. Powders were placed in holes over substrate after being mixed with an amount of bonding. Then, samples were left to dry at

* KASTAMONU UNIVERSITY, FACULTY OF ENGINEERING AND ARCHITECTURE, DEPARTMENT OF MATERIALS SCIENCE AND NANOTECHNOLOGY ENGINEERING, 37000 KASTAMONU, TURKEY

Corresponding author: serkan@kastamonu.edu.tr

100°C temperature for 30 minutes. The operating principle of TIG process system is schematically shown in Fig. 1. The TIG process parameters used in this research are listed as follows: working voltage 20 V, working current 140 A, the travel speed of the nozzle 60 mm/min, the shielding gas flux (Ar) 10 L/min, electrode type W-%2 ThO_2 and the electrode diameter is 2.4 mm.

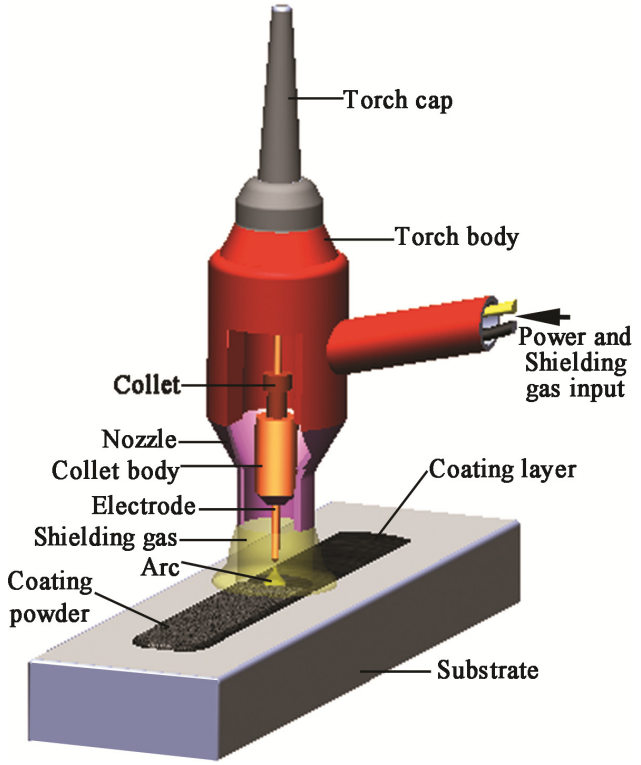

Fig. 1. Schematic diagram of the TIG process system

For microstructure examinations, 10 mm × 10 mm × 10 mm samples were extracted from the middle part of coating material. Coating materials undergoing metallographic procedures were etched in 5 ml HNO_3 + 200 ml HCl + 65 g $FeCl_3$ solution used as etchant for microstructure examinations. While a scanning electron microscope (SEM) and an optical microscope (OM) were used for microstructure examinations, X-ray diffraction (XRD) for and X-ray energy dispersive spectrometer (EDS) were used for phase analyses. Hardness measurements were taken from the top of the coating, in waiting time of 15 second and with a load of 300 gr using a Future-Tech FM 700 brand micro-hardness device.

For wear tests of coatings, reciprocating mode and Ball-on-Flat geometry was used on a CSM Tribometer device (ASTM G133 standard). Wear apparatus was shown in Fig. 2. All tests were carried with 3 N normal load and to obtain 5 cm/s sliding speed, 500 m sliding distance and 7 mm wear trace. Test environment had 25°C temperature and ambient moisture of about 35%. Data collection rate during the tests was selected as 5 Hz. As counter material, spheres of Ø6 mm WC material were used. The tests were carried out at dry conditions and the medium used was air. Worn surfaces were examined with SEM and EDS analysis of samples were conducted.

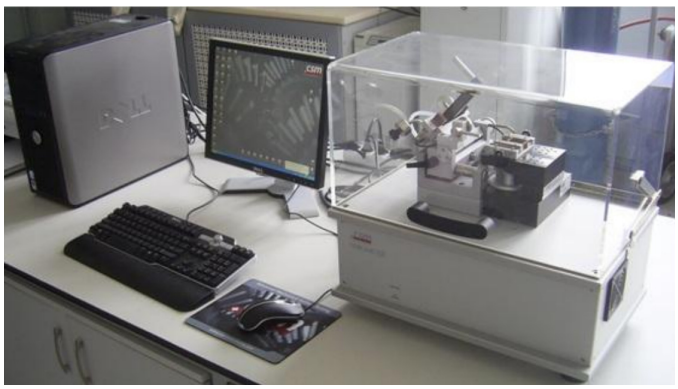

Fig. 2. Wear apparatus (CSM Tribometer)

3. Result and discussion

3.1. Microstructure

The thickness of the FeW/FeW-B_4C coatings produced by TIG was measured as approximately 2 mm using optical microscope. Fig. 3 shows the cross-sectional microstructure of the FeW coating. The rapid directional solidification can be observed at the bonding area of the coating. From the interface to coating surface, cellular and dendritic solidification were observed in opposite direction to the heat flux. On the other hand, the planar solidification was observed at the interface. The structural change is associated with the solidification rate of the metallic liquid in the TIG melt pool and the temperature gradient [11]. As seen in Fig. 3, the FeW coating was well formed without cracking. While the light colored dendrites have 57.71 wt.% W and 42.29 wt.% Fe chemical composition, the dark colored interdendrites eutectic phases have 22.63 wt.% W and 77.37 wt.% Fe composition.

The SEM image of FeW-10 wt.% B_4C coating was shown in Fig. 4. As with FeW coating, the dendritic formation in FeW-10 wt.% B_4C coating was observed. It was understood from the SEM image in Fig. 4 that the borides and carbides formed with the dissolution of B_4C with the given energy. The formation of $Fe_3(C,B)$, $Fe_{23}(C,B)_6$ and FeW_2B_2 phases prove the dissolution of B_4C and this situation is supported with the XRD pattern. The EDS analysis of dark structure in SEM image is 5.81% B, 14.07% W and 80.12% Fe. This analysis demonstrates the formation of FeW_2B_2 phase.

According to Fe-W, Fe-W-C and Fe-C-B binary and ternary phases diagrams [22], the possible products of the reaction between liquid B_4C and FeW may be $Fe_3(C,B)$, $Fe_{23}(C,B)_6$, Fe_2B, α-Fe / $Fe_3(C,B)$, $Fe_{23}(C,B)_6$, Fe_2C, Fe_2W, FeW_3C, FeW_2B_2 etc. XRD patterns of FeW and FeW-10 wt.% B_4C coatings were shown in Fig. 5. While FeW coating has $Fe_2(C,W)$, Fe_3C, FeW_3C and α-Fe phases, FeW-10 wt.% B_4C coating has $Fe_3(C,B)$, $Fe_{23}(C,B)_6$, Fe_2B, α-Fe / $Fe_3(C,B)$, $Fe_{23}(C,B)_6$ and FeW_2B_2 binary/ternary phases. Carbides and borides in α-Fe matrix were found as reinforcement. Whereas FeW powder was converted into Fe and W with the given energy in the melt pool, B4C powder was converted into B and C. A small amount of W_3C hard phase was obtained from the combination of the carbon

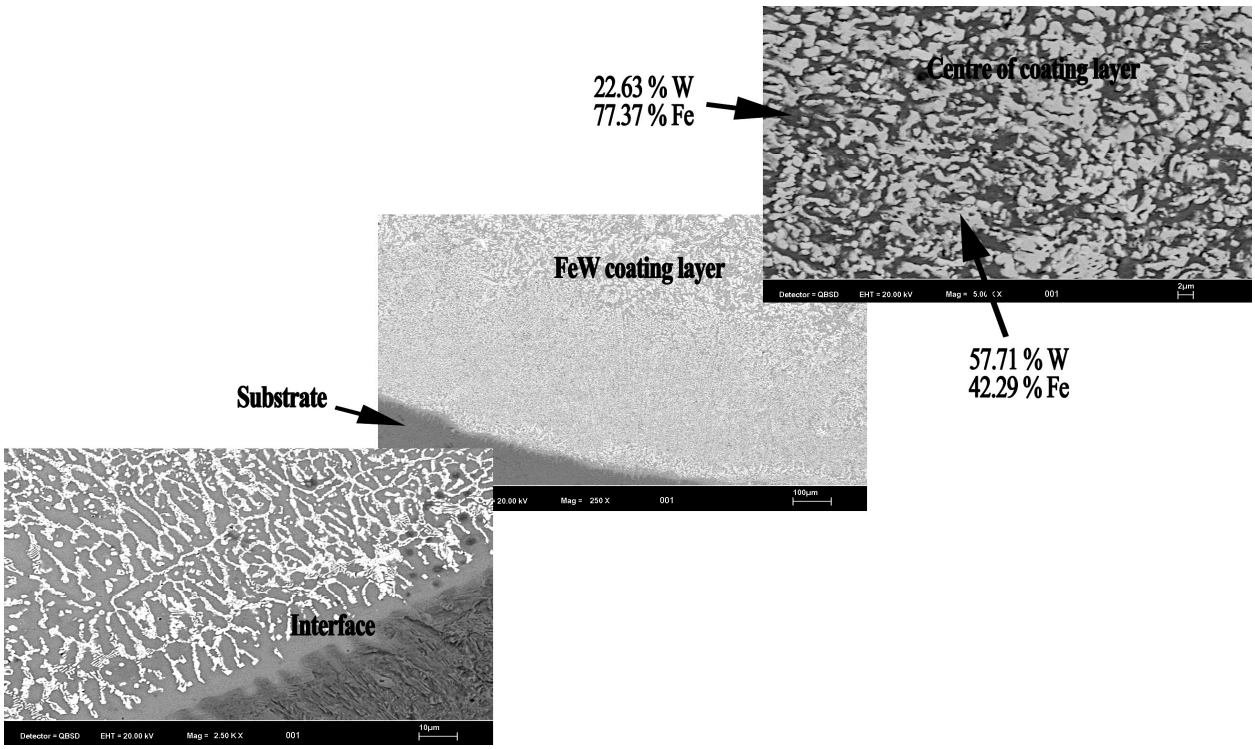

Fig. 3. SEM morphologies and EDS data of FeW coating

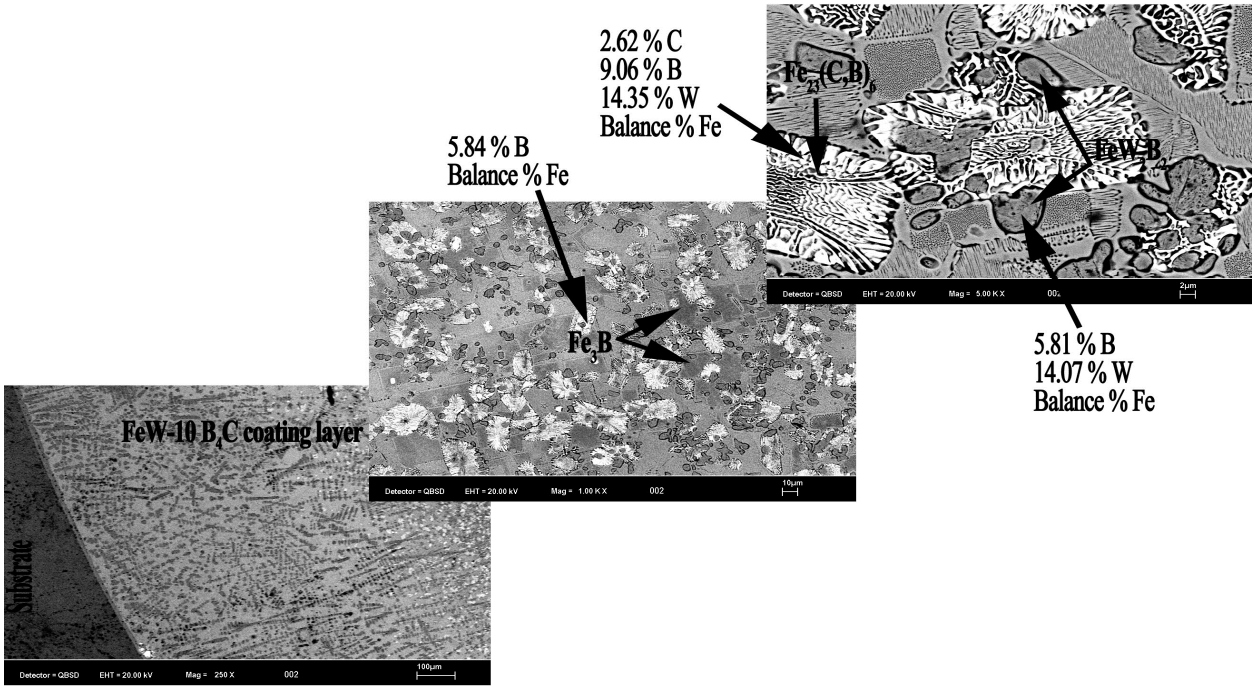

Fig. 4. SEM morphologies and EDS data of FeW-10 B_4C coating

in the substrate and tungsten in the FeW powder. Besides, the unremelted boron carbide ($B_{13}C_2$) phase was observed in the XRD graph. This situation showed that the energy given was not sufficient for dissolving B_4C totally [18].

Hardness graph of substrate (AISI 1060), FeW coating and FeW-10 wt.% B_4C coating was given in Fig. 6. Hardness measurements were taken from the top of the coating. All of the data were an average of five measurements. It was observed that hardness significantly increased. Average hardness values of substrate, FeW coating and FeW-10 wt.% B_4C coating were measured as 205 $HV_{0.3}$, 495 $HV_{0.3}$ and 820 $HV_{0.3}$, respectively. The coatings demonstrates a microhardness 2-4 times higher than the substrate. The carbide and boride formed in microstructure contributed to obtaining microhardness. While the α-Fe matrix provides toughness, the $Fe_{23}(C,B)_6$ phase enhances the strength to the coating layer.

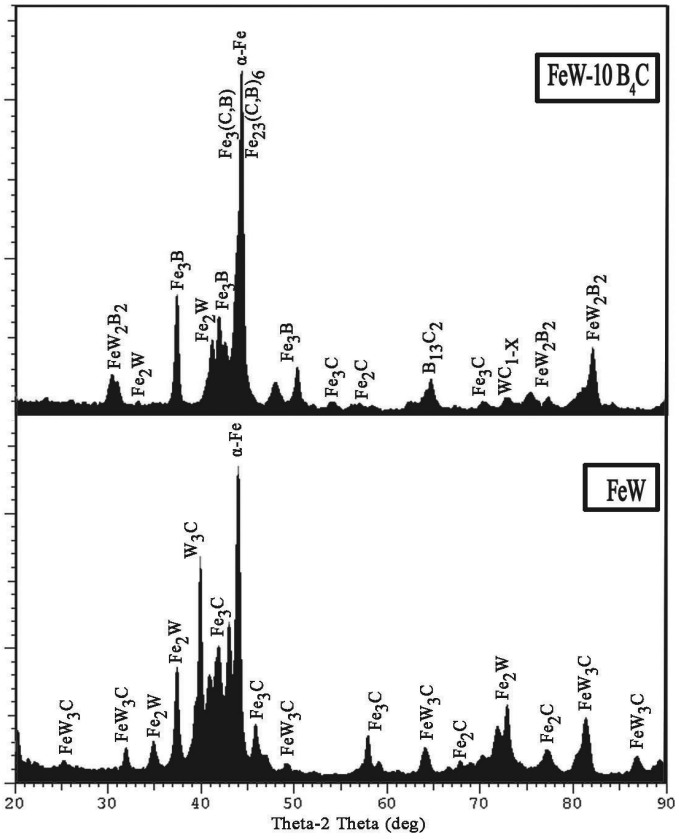

Fig. 5. XRD pattern of coatings

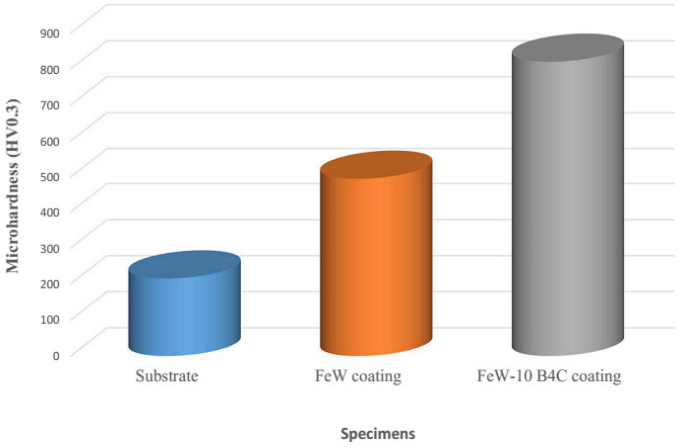

Fig. 6. Hardness graph of substrate and coatings

3.2. Wear

In Fig. 7 the graph of wear rate and coefficient of friction of substrate and coatings were shown. According to graph, the coefficient of friction and wear rate of the coating was very low compared to the substrate. While the coefficient of friction of substrate was ~0.621, the coefficient of friction of FeW coating and FeW-10 wt.% B_4C coating were ~0.512 and ~0.262, respectively. The wear rate of substrate, FeW coating and FeW-10 wt.% B_4C coating were ~4.59×10^{-3} $mm^3/N/m$, ~4.12×10^{-3} $mm^3/N/m$ and ~2.23×10^{-3} $mm^3/N/m$, respectively. Wear resistance of FeW-10 wt.% B_4C coating in comparison to the substrate increased approximately 2 times. This may be attributed to the higher hardness of the coating resulting in lower real area of contact, therefore, smaller number of junctions which require less energy to get sheared during sliding as compared to the substrate. It can also be noted that the friction coefficient of the FeW-10 wt.% B_4C coating is a little smaller than that of the FeW coating. Because B_4C has a lower friction coefficient [11,23], B_4C reduce the contact area of the matrix with the counterface, thus minimizing the smearing effect of the FeW coating on the counterface surface.

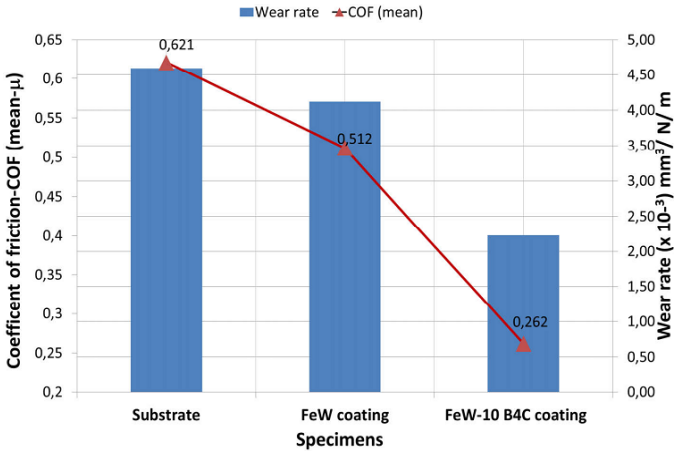

Fig. 7. Coefficient of friction and the wear rate values of the of the substrate and the coatings

Figs. 8-10 shows the worn surface and EDS data of the substrate, FeW coating and FeW-10 B_4C coating, respectively. A longitudinal grooves extending parallel to the sliding direction and plastic deformation are observed inside the wear surface of substrate and FeW coating (Fig. 8 and Fig. 9). When metallic surfaces are in contact during dry sliding wear, the local temperature at the contact points of the surface is high, and the hardness near these points quickly decreases. As a result, serious plastic deformation, local contact-welding between the contacting asperities, and materials transfer lead to serious material removal from the friction surface. It is observed from wear surface of FeW-10 B_4C coating in Fig. 10 that there is a very mild wear with fine scratches for the FeW-10 B_4C coatings, and there is no indication of brittle failure or loose debris formation of B_4C. As mentioned earlier, B_4C particles in the FeW are formed in an in situ manner, which improves the bonding strength between the B_4C particles and FeW interface. Also, EDS data of wear surface of substrate and FeW coating shows that surface of sample after wear occurred oxidation (Fig. 8 and Fig. 9). This oxides have created an effect that reduces coefficient of friction [24].

4. Conclusions

1) FeW and FeW-B_4C coatings on AISI 1060 steel were fabricated using tungsten inert gas (TIG) process. The dendrite structures have been observed from the interface to the

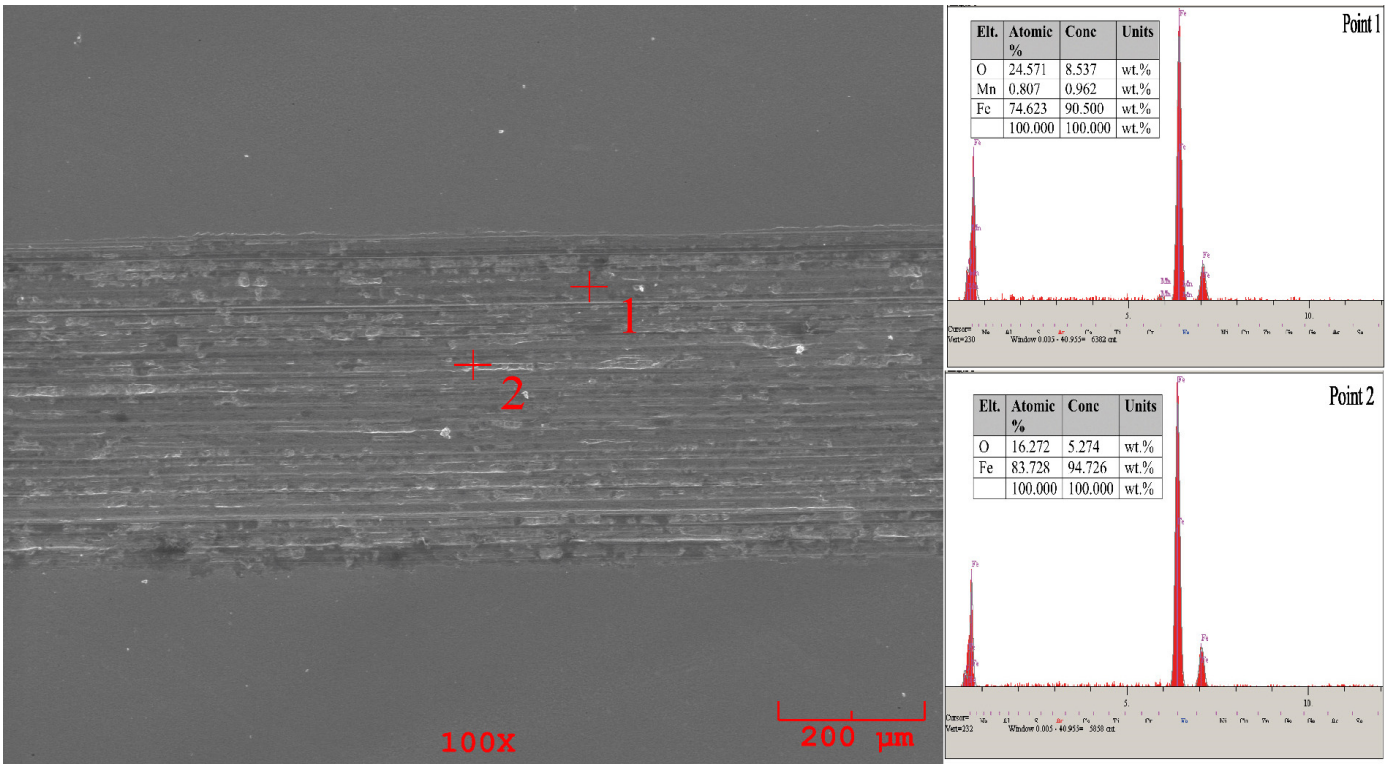

Fig. 8. SEM image and EDS data of worn surface of substrate

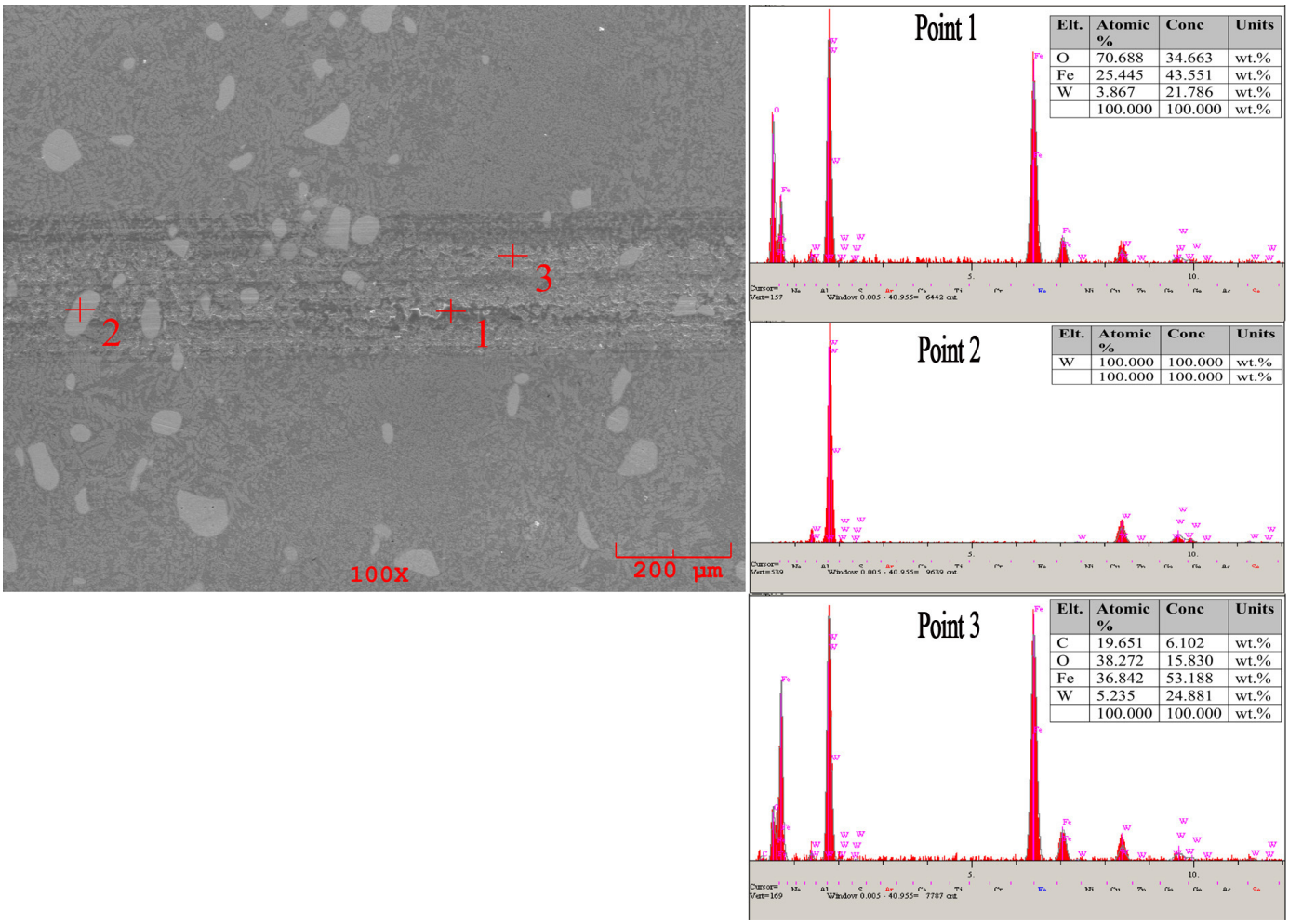

Fig. 9. SEM image and EDS data of worn surface of FeW coating

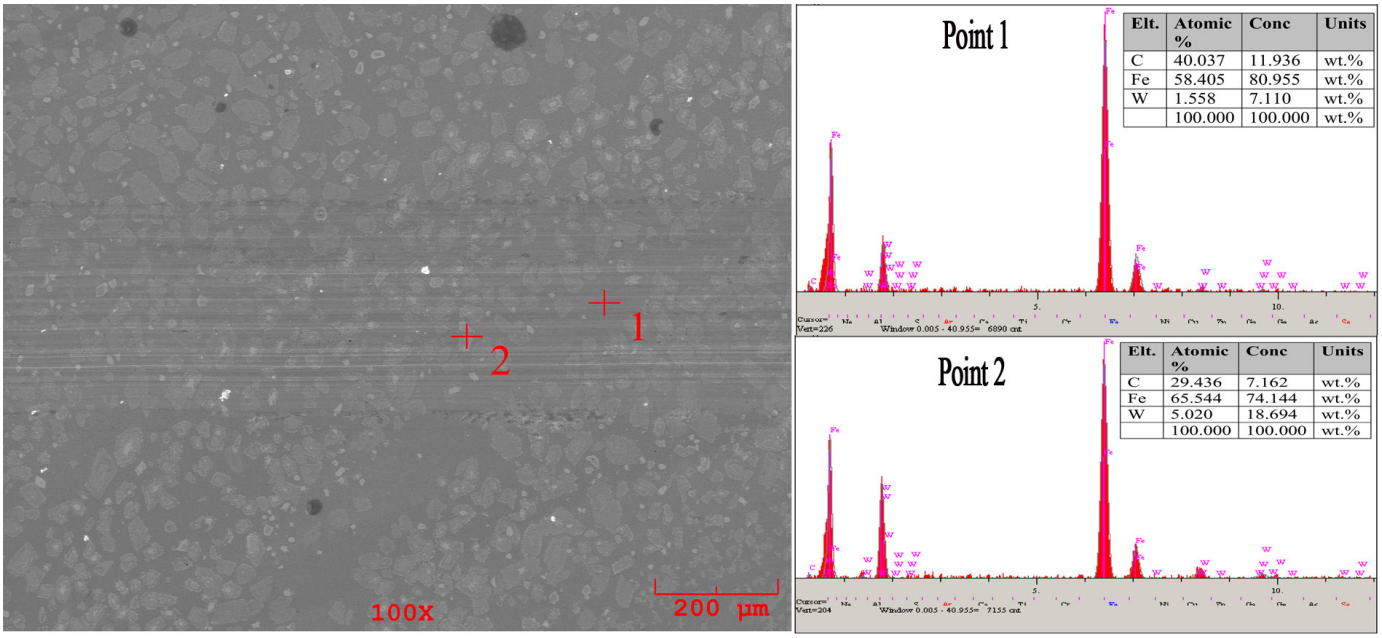

Fig. 10. SEM image and EDS data of worn surface of FeW-10 B_4C coating

coating layer. No evidence of micro crack and gas porosity formation was found on both coating.

2) XRD analysis showed that while the FeW coating consists of $Fe_2(C,W)$, Fe_3C, FeW_3C and α-Fe, the FeW-10 wt.% B_4C coating consists of $Fe_3(C,B)$, $Fe_{23}(C,B)_6$, Fe_2B, α-Fe / $Fe_3(C,B)$, $Fe_{23}(C,B)_6$ and FeW_2B_2 binary/ternary phases.

3) The FeW-10 wt.% B_4C coating revealed higher wear resistance and lower friction coefficient than that of the substrate and FeW coating. SEM images of wear surfaces showed that while a longitudinal grooves and plastic deformation in the substrate and FeW coating are occurred, a very mild wear with fine scratches is occurred in the FeW-10 B_4C coatings.

REFERENCES

[1] X.B. Liu, Y.J. Gu, Materials Letters **60**, 5, 577 (2006).

[2] W. Pang, H.C.Man, T.M. Yue, Materials Science and Engineering A **390**,144 (2005).

[3] S. Islak, Ö. Eski, S. Buytoz, M. Karagöz, J. Stokes, Materials Testing **54**, 11-12, 793 (2012).

[4] S. Islak, M.M. Yıldırım, e-Journal of New World Sciences Academy **4**, 2, 227 (2009).

[5] R. Yazdi, S.F. Kashani-Bozorg, Materials Chemistry and Physics **152**, 147 (2015).

[6] M.M. Yildirim, S. Buytoz, S. Islak, Proceedings of 11th International Materials Symposium, Denizli-Turkey, 258 (2006).

[7] B. Lotfi, M. Rostami, Z. Sadeghian, Transactions of Nonferrous Metals Society of China **24**, 9, 2824 (2014).

[8] S. Lu, O. Kwon, Y. Guo, Wear **254**, 421 (2003).

[9] B. Lou, Z. Chen, W. Bai, G. Dong, Transactions of Nonferrous Metals Society of China **16**, 643 (2006).

[10] R. Sathiskumar, N. Murugan, I. Dinaharan, S.J. Vijay, Archives of Metallurgy and Materials **59**, 1, 83 (2014).

[11] M. Chao, X. Niu, B. Yuan, E. Liang, D. Wang, Surface and Coatings Technology **201**, 1102 (2006).

[12] S. Buytoz, M. Ulutan, B. Kurt, S. Islak, İ. Somunkıran, e-Journal of New World Sciences Academy **5**, 1, 35 (2010).

[13] S. W. Huang, M. Samandi, M. Brandt, Wear **256**, 1095 (2004).

[14] M.A. Maleque, B.A. Ghazal, M.Y. Ali, M. Hayyan, A.S. Ahmed, International Conference on Functional Materials and Metallurgy, ICoFM 2014, 17 (2014)

[15] B. Du, Z. Zou, X. Wang, S. Qu, Applied Surface Science **254**, 6489 (2008).

[16] G. Sun, Y. Zhang, C. Liu, K. Luo, X. Tao, P. Li, Materials & Design **31**, 2737 (2010).

[17] Y.P. Kathuria, Surface and Coatings Technology **140**, 195 (2001).

[18] W. Xibao, Applied Surface Science **252**, 2021 (2005).

[19] W. Rafainello, M. Srivinasan, Non-Oxide Materials: Applications and Engineering, in Carbide, Nitride, and Boride Materials Synthesis and Processing, Chapman-Hall, London, (1997).

[20] M.T. Spohn, Minerals Review **6**, 113 (1994).

[21] H.O. Pierson, Handbook of Refractory Carbides and Nitrides, William Andrew Pub., Noyes, (1996).

[22] P. Villars, A. Prince, H. Okamoto, Handbook of Ternary Alloy Phase Diagrams, ASM International, Materials Park, OH, (1995).

[23] E.B. Clark, B. Roebuck, International Journal of Refractory Metals and Hard Materials **11**, 23 (1992).

[24] G.B.V. Kumar, C.S.P. Rao, N. Selvaraj, Journal of Minerals & Materials Characterization & Engineering **10**, 1, 59 (2011).